Biosensors and Bioelectronics 38 (2012) 67–73

Contents lists available at SciVerse ScienceDirect

Biosensors and Bioelectronics

journal homepage: www.elsevier.com/locate/bios

Rapid detection of avian influenza H5N1 virus using impedance measurement of immuno-reaction coupled with RBC amplification

Jacob Lum [a,b], Ronghui Wang [c], Kentu Lassiter [b], Balaji Srinivasan [d], Daad Abi-Ghanem [e], Luc Berghman [e], Billy Hargis [a,b], Steve Tung [d], Huaguang Lu [f], Yanbin Li [a,b,c,*]

[a] Cell and Molecular Biology Program, University of Arkansas, Fayetteville, AR 72701, USA
[b] Department of Poultry Science, University of Arkansas, Fayetteville, AR 72701, USA
[c] Department of Biological and Agricultural Engineering, University of Arkansas, Fayetteville, AR 72701, USA
[d] Department of Mechanical Engineering, University of Arkansas, Fayetteville, AR 72701, USA
[e] Departments of Poultry Science and Veterinary Pathobiology, Texas A&M University, College Station, TX 77843, USA
[f] Animal Diagnostics Laboratory, Pennsylvania State University, University Park, PA 16801, USA

ARTICLE INFO

Article history:
Received 28 March 2012
Accepted 30 April 2012
Available online 8 May 2012

Keywords:
Avian influenza
AI H5N1
Impedance measurement
Interdigitated microelectrode
Immunosensor
Virus detection

ABSTRACT

Avian influenza virus (AIV) subtype H5N1 was first discovered in the 1990s and since then its emergence has become a likely source of a global pandemic and economic loss. Currently accepted gold standard methods of influenza detection, viral culture and rRT-PCR, are time consuming, expensive and require special training and laboratory facilities. A rapid, sensitive, and specific screening method is needed for in-field or bedside testing of AI virus to effectively implement quarantines and medications. Therefore, the objective of this study was to improve the specificity and sensitivity of an impedance biosensor that has been developed for the screening of AIV H5. Three major components of the developed biosensor are immunomagnetic nanoparticles for the separation of AI virus, a microfluidic chip for sample control and an interdigitated microelectrode for impedance measurement. In this study polyclonal antibody against N1 subtype was immobilized on the surface of the microelectrode to specifically bind AIV H5N1 to generate more specific impedance signal and chicken red blood cells (RBC) were used as biolabels to attach to AIV H5N1 captured on the microelectrode to amplify impedance signal. RBC amplification was shown to increase the impedance signal change by more than 100% compared to the protocol without RBC biolabels, and was necessary for forming a linear calibration curve for the biosensor. The use of a second antibody against N1 offered much greater specificity and reliability than the previous biosensor protocol. The biosensor was able to detect AIV H5N1 at concentrations down to 10^3 EID_{50} ml^{-1} in less than 2 h.

1. Introduction

Avian influenza viruses (AIV) are a considerable health problem for both humans and animals. One AIV subtype, H5N1, has been shown to infect wild birds, domestic poultry and mammals, including humans, with deadly effects. First discovered in 1997 in Hong Kong, H5N1 has spread throughout much of south Asia and parts of Europe and Africa (Peiris et al., 2007). The virus has a high mortality rate in both poultry and humans, often having a 100% mortality rate in poultry flocks and a 60% mortality rate in humans, with 587 reported human cases and 346 deaths since 2003 (WHO, 2011). In addition to the health impact of AIV H5N1, the possible economic impact stands to be massive. Already AIV H5N1 is estimated to have cost the poultry industry over $10 billion dollars and the World Bank has estimated that a severe outbreak in humans would cost upwards of $3.13 trillion to the global economy (Burns et al., 2008). Rapid detection and identification of H5N1 is crucial to controlling outbreaks (MacKay et al., 2008). Definitive answers from a laboratory may take 2–3 days, during which time the virus may be allowed to spread. For this reason, a rapid, specific and in-field method of detection for AIV H5N1 is needed.

Current gold standard methods of AIV detection, viral isolation culture and rRT-PCR, are time-consuming, expensive and require special training and facilities (Charlton et al., 2009; Ellis and Zambon, 2002). Other techniques of AIV detection, such as ELISA and immunochromatographic strips, lack the specificity and sensitivity required. Biosensors, which combine a biological sensing element, a transducer, and a signal processing unit, have shown promise in the fields of food safety, drug development, environmental monitoring, healthcare, and pathogen detection

* Correspondence to: Department of Biological and Agricultural Engineering, University of Arkansas, 203 Engineering Hall, Fayetteville, AR 72701, USA. Tel.: +1 4795752881; fax: +1 4795752846.
E-mail address: yanbinli@uark.edu (Y. Li).

0956-5663/$ - see front matter © 2012 Elsevier B.V. All rights reserved.
http://dx.doi.org/10.1016/j.bios.2012.04.047

(Amano and Cheng, 2005). Several types of biosensors, such as surface plasmon resonance (SPR), quartz crystal microbalance (QCM) and optical interferometric, have been researched as alternatives to conventional detection methods for avian influenza virus, but while the developed biosensors have shown potential, they lack subtype specificity and many are not practical for use in the field (Estmer-Nilsson et al., 2010; Sato et al., 1996; Peduru Hewa et al., 2009; Xu et al., 2007).

Impedance biosensors, which rely on electrochemical changes in the electrode environment to detect an analyte, have advantages over traditional detection methods of AIV due to their simple design, relatively low cost and ease of miniaturization (Pejcic et al., 2006). Impedance biosensors can be combined with interdigitated microelectrode arrays (IDAMs) to overcome many of the problems that occur with macroelectrodes. IDAMs offer the desired features of low ohmic drop, fast establishment of steady-state, rapid reaction kinetics, increased signal to noise ratio, small sample sizes and reduced detection time due to their low response time (Varshney and Li, 2009). The use of microfluidic devices in biosensors has also shown promise in the field of pathogen detection, offering a high surface-to-volume ratio, the ability to precisely control small volumes of sample and lower detection time (Yager et al., 2006). When coupled with microbial detection methods, immunomagnetic separation can provide several advantages over traditional isolation techniques. Immunomagnetic separation is simple, provides high capture efficiency and specificity, can be used to concentrate a sample for more sensitive detection and requires no expensive equipment or special training (Horak et al., 2007).

A Faradic impedance biosensor for the detection of AIV was studied using an open interdigitated array microelectrode with immobilized polyclonal antibody against H5 and RBC amplification (Wang et al., 2009). The developed biosensor had a lower detection limit of 10^3 EID_{50}/ml and was only specific to the H5 antigen. Another biosensor system was developed for AIV detection using a microfluidic biochip with an embedded microelectrode array combined with immunomagnetic separation (Li et al., 2006; Wang et al., 2007). In their research anti-H5 antibody-coated nanobeads were used to isolate the virus and the impedance of the sample was measured using the microfluidic biochip with no antibody immobilized to the microelectrode. Their result showed that the lower detection limit was 10^3 EID_{50}/ml for detection of AIV H5.

In this study, we describe an improved non-Faradic impedance biosensor using a second antibody against N1 subtype, RBC biolabels and an interdigitated microelectrode array embedded in a microfluidic biochip for the specific detection of AIV H5N1. A sample of AIV was isolated using immunomagnetic nanobeads coated in monoclonal antibody against H5. The microelectrode surface was modified using Protein A (*Staphylococcus aureus*) and then polyclonal antibody against N1 was immobilized. Target AIV H5N1 was bound to the antibody on the microelectrode surface, causing a change in impedance compared to a control sample. RBCs were used as biolabels to amplify the impedance change through their binding to the AIV on the microelectrode. RBCs were used as biolabels to amplify the antibody-virus binding due to their larger diameter (7–12 μm) compared to the virus (80–120 nm), and strong and specific binding by virus hemagglutinin to sialic acid linkages found on the cell surface (Cell Size Database, 2012; Suarez and Schultz-Cherry, 2000; Lamb and Krug, 2001; Murphy and Webster, 1996). Both the virus and the RBC act as resistors in the system, and the RBC has a larger resistive value due to its larger size compared with the virus. Non-target influenza subtypes were used to test the specificity of the biosensor. Transmission electron microscopy and atomic force microscopy were used to confirm the binding of AIV H5N1 and RBCs.

2. Materials and methods

2.1. Materials

Phosphate buffered saline (PBS, 10 mM, pH 7.4), bovine serum albumin (BSA) and Protein A (*S. aureus*) were purchased from Sigma-Aldrich (St. Louis, MI). Protein A and BSA were both reconstituted in PBS. Washing solution (20 ×; 0.04M imidazole buffered saline with 0.4% Tween 20) was purchased from KPL Inc. (Gaithersburg, MD) and diluted with Milli-Q water (Milli-Q, 18.2 MΩ cm, Bedford, MA) to 1:200,000 dilution for use as a measuring buffer. Monoclonal mouse antibody against H5 and polyclonal rabbit antibody against N1 were provided by Dr. Luc Berghman's research laboratory (Department of Poultry Science, Texas A&M University). Chicken red blood cells suspended in isotonic dextrose at a concentration of 0.5% (w/v) were obtained from the Poultry Health Lab (University of Arkansas, Fayetteville, AR). Magnetic streptavidin-coated 30 nm nanobeads were acquired from Ocean NanoTech (Springdale, AR). The nanobeads were used at a concentration of 0.5 mg ml^{-1}.

Avian influenza A/H5N1 (Scotland 59) was provided by the USDA/APHIS National Veterinary Services Lab (Ames, IA). The virus was inactivated by the USDA with β-propiolactone, eliminating viral infectivity while preserving hemagglutination activity (Goldstein and Tauraso, 1970). The stock concentration of the virus was 10^7 EID_{50} ml^{-1} or the equivalent HA titer of 128. Non-target influenza virus subtypes were provided by Dr. Huaguang Lu (Animal Diagnostics Laboratory, Pennsylvania State University, University Park, PA). All non-target virus subtypes were used at an HA titer of 128.

2.2. Microfluidics biochips with embedded interdigitated microelectrodes

A microfluidics biochip with an embedded gold interdigitated array microelectrode was fabricated by Dr. Steve Tung's laboratory (University of Arkansas, Fayetteville, AR). A microfluidic channel (40 μm deep and 100 μm wide) with an oval-shaped microfluidics chamber (40 μm deep, 500 μm wide and 1723 μm long; 34.5 nl volume) was molded from PDMS and fixed to an interdigitated microelectrode chip. Each electrode consisted of 25 pairs of 10 μm wide electrode fingers spaced 10 μm apart.

2.3. AIV H5 separation with antibody-coated 30 nm magnetic nanobeads

Monoclonal mouse antibody to H5 was biotinylated using sulfo-NHS-biotin and purified using a Slide-A-Lyzer dialysis kit from Pierce Protein Research Product (10K MWCO, Rockford, IL). The antibody was diluted to a concentration of 260 μg ml^{-1}. Thirty-three microliters of 30 nm magnetic nanobeads (0.5 mg ml^{-1}) was washed with 250 μl of PBS and resuspended in 67 μl of PBS. The nanobeads were mixed with 67 μl of the antibody for 30 min in a rotating mixer. The nanobead-antibody conjugates were separated using a magnet for 30 min, washed with 150 μl of PBS and resuspended in 67 μl of PBS. The conjugates were added to 67 μl of virus sample and incubated for 45 min at 37 °C, forming nanobead–antibody–AIV complexes. The complexes were separated with a magnet for 1 h and the rest was removed. The complexes were washed with 150 μl of measuring buffer and separated with a magnet for 1 h and the waste was removed. The complexes were resuspended in 150 μl of measuring buffer and stored at 4 °C for further impedance measurement.

2.4. Modification of microelectrodes and AIV detection

The experimental protocol consisted of three elements: electrode surface modification, AIV detection and RBC amplification. After each immobilization/binding step, the microfluidic chamber was flushed with measuring buffer at a pumping rate of 1 ml h^{-1} to wash away any unbound particles and the impedance was measured. After washing the pump was stopped for 2 min and then impedance was measured. The modification of the electrode surface was done using Protein A, a cell surface protein found in Staphylococcus aureus that can form stable complexes with Au through van der Waal interaction ($K_a \sim 10^8$ M^{-1}) and contains five tandem domains that bind the Fc region of IgG with high affinity and selectivity (Bohinski, 2000; Lindmark et al., 1983). Protein A (1 mg ml^{-1}) was allowed to adsorb directly onto the gold surface of the microelectrode for 1.5 h. Polyclonal antibody against N1 (270 μg ml^{-1}) was incubated for 2 h and immobilized through Protein A's affinity towards the F_c region of antibodies. Because Protein A specifically binds the F_c region and the F_{ab} region (antigen-binding) is orientated away from the electrode surface, resulting in efficient antibody–antigen binding (Boltovets et al., 2002). Protein A-antibody binding and anti-N1 activity were tested using Dot-ELISA. BSA (1%) was incubated for 30 min to block any non-specific binding sites on the electrode surface.

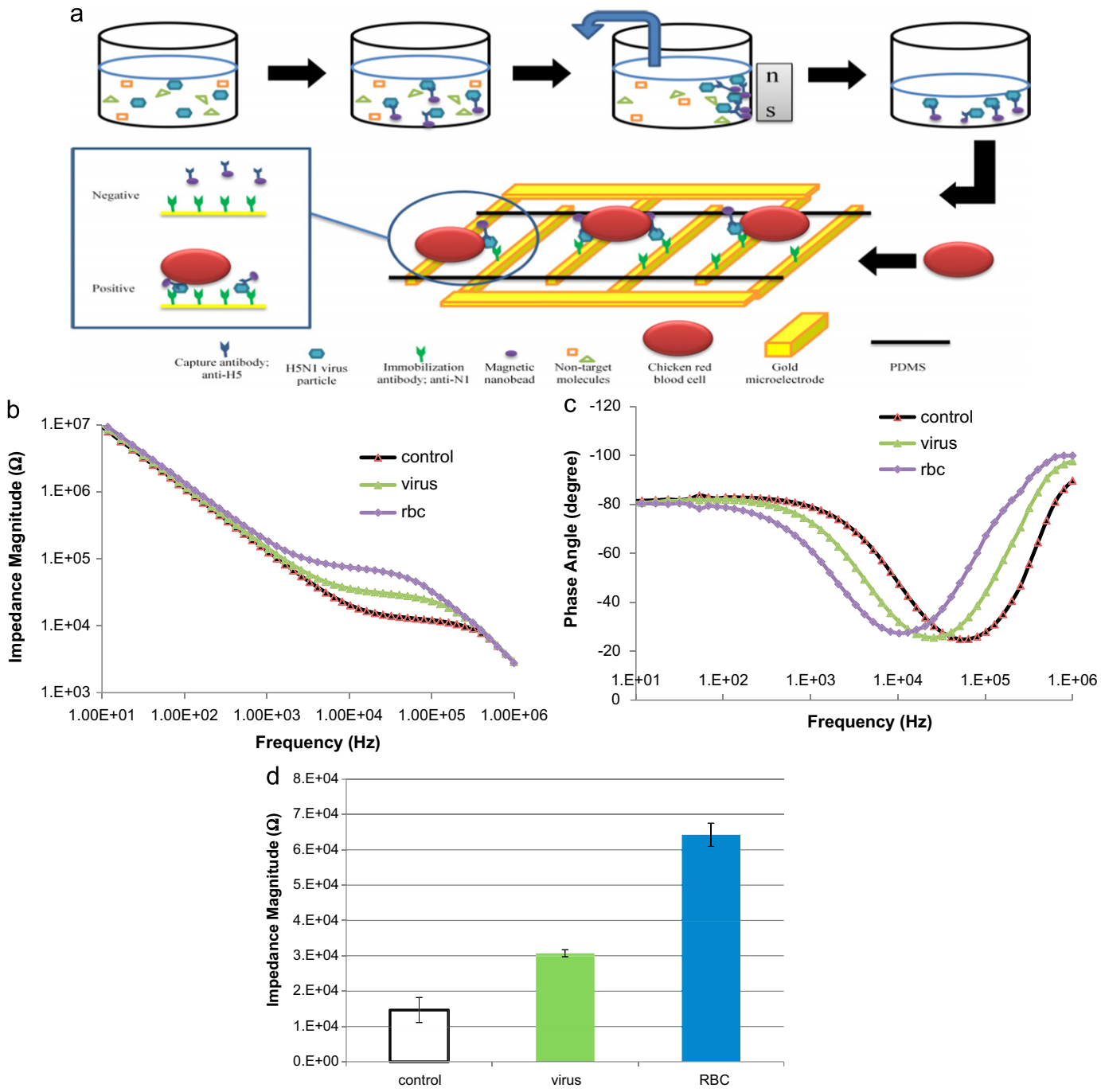

Fig. 1. (a) Biosensor design based on immunomagnetic separation and concentration, microfluidics channel with interdigitated microelectrode array with immobilized second antibody and red blood cell amplification. Impedance magnitude (b) and phase angle (c) of control sample (beads and antibody only), H5N1 sample (10^5 EID_{50} ml^{-1}) immobilization and RBC (0.5%) biolabeling in the frequency range from1 Hz to 1 MHz. Amplitude of voltage, 100 mV. (d) Impedance magnitudes measured at 25.8 kHz for control sample (beads and antibody only), H5N1 sample (10^5 EID_{50} ml^{-1}) immobilization and RBC (0.5%) biolabeling.

A control sample of nanobead/antibody complexes with no virus was incubated in the microfluidic chamber for 30 min. An AIV sample previously prepared by immunomagnetic separation was incubated in the microfluidic chip for 30 min. A 0.5% (w v^{-1}) solution of RBCs was incubated in the microfluidic chamber for 30 min to allow for binding of the RBCs with the captured virus for amplification of the impedance signal. Though RBCs can be bound by all subtypes of influenza viruses, the immunomagnetic separation step using monoclonal antibody against H5 immobilized on the nanobeads and the antibody against N1 immobilized on the electrode surface ensured the specificity of the biosensor for AIV H5N1.

Impedance measurements were done using an IM-6 impedance analyzer with the IM-6/Thales 2.49 software (BAS, West Lafayette, IN). Test-sense and counter-reference probes were connected to the interdigitated microelectrode array with connecting wires. In all impedance measurements a sinusoidal AC potential of 100 mV was applied. 100 mV was used in the study to overcome noise while impedance is still linearly measured (Varshney et al., 2007). Impedance magnitude and phase angle were measured at 54 points in the frequency range from 1 Hz to 1 MHz. All impedance measurements were done in the presence of measuring buffer.

2.5. AFM and TEM

Atomic force microscopy (AFM) was used to confirm the binding of AIV H5N1 and RBC biolabels onto the microelectrode surface. Samples for AFM were prepared by following the electrode modification protocol and allowing the sample to air dry in a fume hood. AFM imaging was done using a Nanoscope III AFM (Digital Instruments, Santa Barbara, CA). Image analysis was done using Gwyddion data visualization and analysis software (version 2.23).

For TEM sample preparation, a drop of magnetic nanobeads with or without target virus was added on a formvar-carbon coated nickel grids and then air dried in a fume hood. TEM imaging was done using JEOL 100CX.

2.6. Statistical analysis

Microsoft Excel (Microsoft, Redmond, VA) was used for statistical analysis of all data, including determination of means and standard deviation, as well as *t*-tests.

3. Results and discussion

3.1. Characterization of the impedance spectrum data

The impedance magnitude of each step in the modification of the electrode surface and detection of AIV H5N1 with RBC biolabels was recorded in a Bode plot as shown in Fig. 1(B). The binding of virus onto the electrode surface caused an increase in the impedance magnitude compared to the control sample, with the RBC biolabels further amplifying the impedance change. Maximum change in impedance magnitude was seen in the mid-frequency range, 1–50 kHz. The phase angle was also recorded for all impedance measurements as shown in Fig. 1(C). The phase angle describes the contributions of the resistive and capacitive portions to the impedance magnitude. A current passing through a capacitor is phase shifted by -90° with respect to the voltage while a current passing through a resistor will be in phase with the voltage, therefore having a phase angle of 0°. The dip in the phase angle in the mid-frequency range indicates where the capacitive portion of impedance contributes the least to the impedance measurement. The phase angle is close to -90° on both ends of the impedance spectrum while it approaches 0° in the middle frequency range. From this, it can be concluded that the capacitive portion of impedance is dominant at the high and low ends of the frequency range while the resistance dominates the mid frequency range, where the largest amount of impedance magnitude change is seen. This is consistent with the previous biosensor design using a microfluidic biochip.

Simulations with an equivalent circuit model were used to better understand the impedance data. The equivalent circuit used is shown in Fig. 2(a). The circuit consists of the resistance of the solution (R_s), resistance of the PDMS (R_p), double layer capacitance (C_{dl}), and geometric capacitance (C_g). The R_s component of the circuit represents the resistance of the bulk electrolyte solution. The R_p component accounts for the resistance of the PDMS layer connecting the electrode fingers (Duffy et al., 1998; Chen et al., 2008). The C_{dl} component represents the effect of ions near the surface of the electrodes and the C_g component represents the capacitance of the solution.

Fig. 2(b) shows the experimental data compared to the simulated data generated using the equivalent circuit. The equivalent circuit was validated using the IM-6/Thales software. The software selected 54 points from the experimental data to fit a simulated impedance spectrum. The mean error of the impedance magnitude was 2.4% with a maximum error of 13%. The mean error of the phase angle was 0.9° with a maximum error of 11.3°.

The equivalent circuit can be used to understand better the components affecting the impedance spectrum. As stated in Section 3.1, the capacitive portion of impedance dominates at the high and low ends of the frequency range while the resistance dominates the mid-frequency range. All maximum changes in impedance were located in the frequency range of 1–50 kHz,

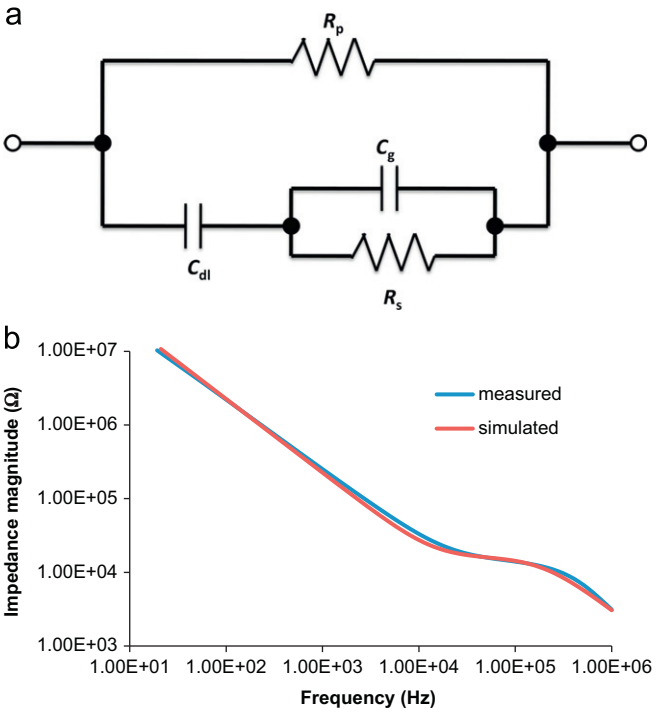

Fig. 2. (a) Equivalent circuit used for data analysis. The equivalent circuit components were resistance of the solution (R_s), resistance of PDMS (R_p), double layer capacitance (C_{dl}), and geometrical capacitance (C_g). (b) Bode diagram of measured impedance data and simulated impedance data generated by curve fitting of equivalent circuit. Measured data taken with 10^5 EID_{50} ml^{-1}H5N1 virus sample.

indicating that R_s contributed the greatest amount to the impedance change. The frequency ranges below 1 kHz and above 50 kHz showed no significant impedance change ($P > 0.05$) between the detection steps and so it can be assumed that the capacitance contributed little to the impedance change. This was confirmed by examining the simulated values by curve fitting the experimental data of the control, virus, and RBC amplification steps shown in Table 1. The percent change in R_s between the control and virus was 155%, while the change in C_{dl} was −26.8%. The percent changes in R_s and C_{dl} between the control and RBC amplification were 461% and 33.3%, respectively, confirming that the majority of the impedance magnitude change between detection steps was due to a change in the resistance of the solution. When only the R_s value is looked at the biosensor can detect H5N1 down to a concentration of 10^2 EID_{50} ml^{-1} and change in R_s can be strongly correlated ($R^2 = 0.98$; $y = 10.47 \times -1.599$) with virus concentration after RBC biolabeling between the concentrations of 10^5 and 10^1 EID_{50} ml^{-1}. The lower detection limit using R_s values was determined by multiplying the standard deviation of the control R_s values by 3 and was found to be 10^2 EID_{50} ml^{-1} when using RBC biolabels.

Table 1
Simulated values of R_s and C_{dl} in the equivalent circuit for the control, virus and RBC amplification steps with the percent change between two steps.

Detection step	C_{dl} (nF)		R_s (kΩ)	
	Value (nF)	Change (%)	Value (kΩ)	Change (%)
Control	1.644		13.14	
Virus	1.203	−26.8%	33.49	155%
RBC	1.095	−33.3%	73.75	461%

The impedance value increased with the virus captured on the electrode surface, as opposed to the value reported by Wang et al. (2007) where the presence of virus decreased the impedance value. This can explain which action is causing the impedance change. The impedance change caused by the presence of the virus in the (Wang et al., 2007) biosensor was caused by a binding of the charged antibodies by the virus, thus changing the electrochemistry of the sensing environment whereas in the described biosensor the formation of the protein biolayer on the electrode surface inhibited the flow of ions between the electrode fingers.

3.2. Binding of AIV virus and RBC

The SEM images of magnetic nanobeads coated with the antibody, an AIV and their binding are shown in Fig. 3 (a–c). It was estimated that more than ten magnetic nanobeads could bind to a single virus particle, depending upon their concentrations. Fig. 3(d) shows an image of the binding of RBCs on the AIVs captured on the surface of gold interdigitated microelectrode. The AFM images of two virus particles captured on the microelectrode

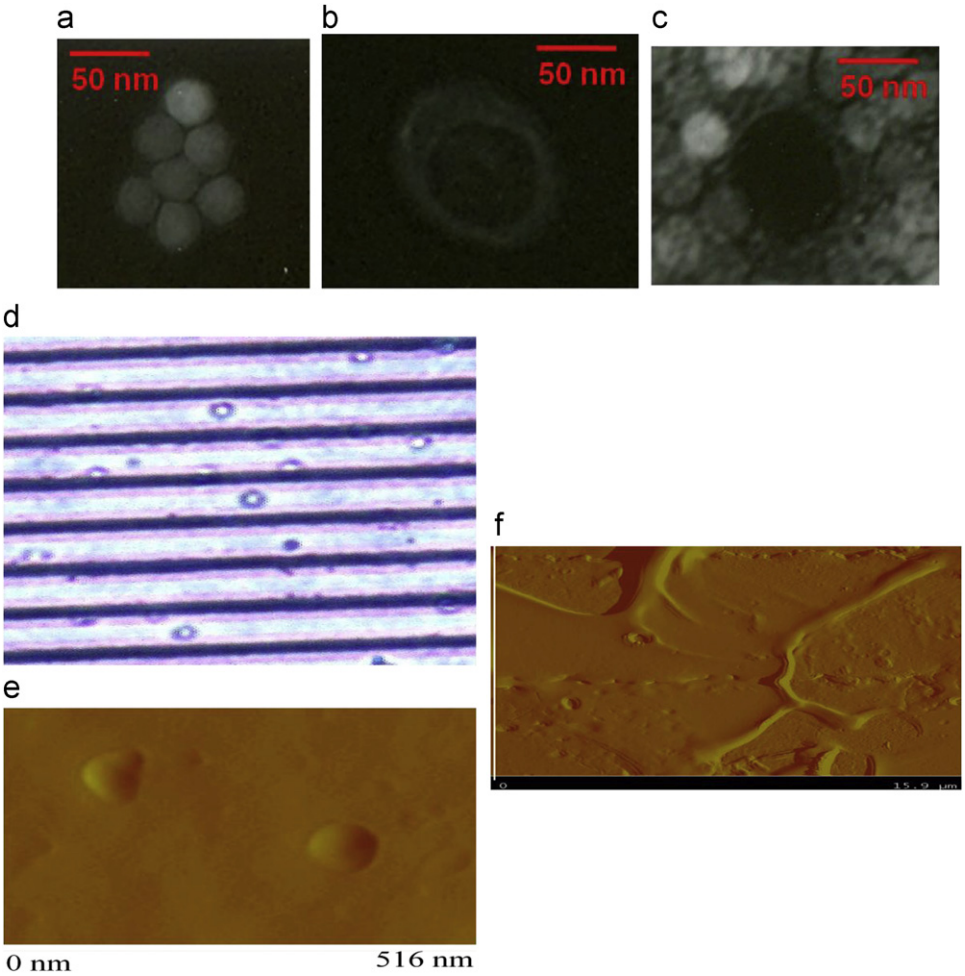

Fig. 3. (a) TEM micrographs of 30 nm magnetic nanobeads (100,000 ×); (b) inactivated avian influenza virus H5N1 (100,000 ×) and (c) 30 nm nanobeads captured H5N1 viruses (100,000 ×). (d) Red blood cells (RBCs) bound to captured AIV on the microelectrode surface. (e) AFM microscopy of AIV H5N1 virus captured on the microelectrode surface. (f) AFM microscopy of a single RBC bound to captured virus on the microelectrode surface.

surface and the binding of a RBC on the AIV are shown in Fig. 3 (e) and (f). The shape of RBC was deformed due to dehydration and washing procedure. These TEM and AFM images clearly demonstrate the binding of AIV with the magnetic nanobeads and the microelectrode and the binding of RBC with AIV.

3.3. Detection of AIV H5N1 with RBC

In Fig. 4(a) the impedance magnitude at 25.8 kHz was plotted for each step in the procedure for detecting 10^5 EID_{50} ml^{-1} of AIV H5N1. The frequency of 25.8 kHz was found to have the highest R^2 value in the frequency range of 1–50 kHz. Nanobead/antibody conjugates without target H5N1 virus were subjected to the same treatment as that of the sample, and was used as a control. Capture of the virus onto the electrode surface by the immobilized antibody against N1 resulted in a large impedance increase (16 kΩ), with virus binding of the RBC biolabel further amplifying the impedance change (34 kΩ).

Triplicate tests were conducted for each virus concentration in the range 10^1–10^5 EID_{50} ml^{-1} to determine the effect of virus concentration on impedance change. No linear relationship (R^2 = 0.10) between virus concentration before RBC biolabeling and change in impedance magnitude was seen in the range of virus concentration 10^1 EID_{50} ml^{-1}–10^5 EID_{50} ml^{-1} and the detection limit was shown to be 10^5 EID_{50} ml^{-1}. After RBC biolabeling, a linear relationship ($\Delta Z = 8562.3c_{virus} - 5212.4$; $R^2 = 0.83$) between virus concentration and impedance magnitude change was found in the range of virus concentration from 10^1 to 10^5 EID_{50} ml^{-1}. The lower detection limit was determined by multiplying the standard deviation of the control measurements by 3 and was found to be 10^3 EID_{50} ml^{-1} when using RBC biolabels.

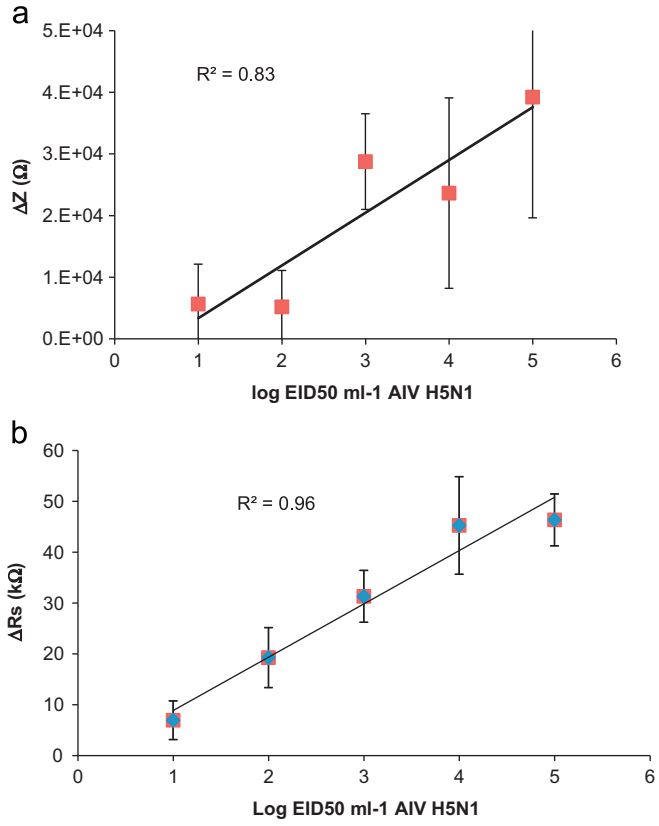

Fig. 4. (a) Linear relationship between the logarithmic value of the AIV H5N1 concentration and change in impedance magnitude after RBC biolabeling at 25.8 kHz. (b) Linear relationship between the logarithmic value of the AIV H5N1 concentration and change in R_s value after RBC biolabeling.

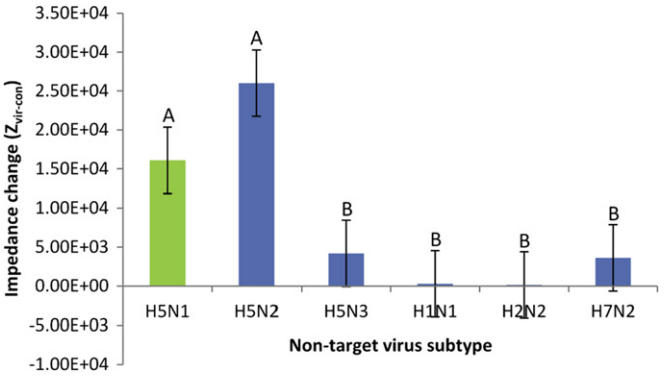

Fig. 5. Change in impedance magnitude between controls and non-target influenza virus treatments at 25.8 kHz in comparison with target AIV H5N1. Concentration of H5N1 subtype was 1.28 HA titer while concentration of non-target viruses was 128 HA titer. The means and error bars (standard deviation) were calculated based on 3 replicates.

3.4. Specificity of the detection

The immunosensor was evaluated for specificity with five different subtypes of avian influenza viruses using the same procedure described previously. False positives from antibody cross-reactivity and non-specific binding were of main concern. Several non-target viruses were chosen due to the overlapping antigenic properties of their HA and NA surface proteins, containing either H5 or N1, to test for any cross-reactivity of the antibodies. As in the previous case, the frequency point of 25.8 kHz was chosen for evaluation of the specificity tests. Fig. 5 shows the impedance magnitude of each virus subtype measured at 25.8 kHz. Of the five viruses, only subtype H5N2 produce a significant positive signal. The false positive generated by the non-target H5N2 was likely to be due to cross-reactivity of the polyclonal α-N1 antibody immobilized on the microelectrode surface with the N2 protein on the virus surface. N1 and N2 share almost 50% homology with each other, making it likely for some antibodies in a polyclonal batch tobind to the conserved regions between the two. False positives due to non-specific binding to N2 could be reduced by using monoclonal antibodies tested specifically for cross-reactivity with N2.

4. Conclusion

The objective of this study was to determine the effectiveness of using a second antibody against N1 and RBC amplification in improving the specificity and lowering the detection limit of an impedance biosensor for AIV H5N1. The specificity of the biosensor was improved compared to the previous biosensor, which was specific only to H5, by using a second antibody against N1 subtype. Tests with AIV H5N1 and non-target influenza subtypes showed that the biosensor was able to specifically detect subtype AIV H5N1 by both the HA and NA antigens using an immunomagnetic separation step with α-H5 antibodies and an immobilization step with α-N1 antibodies, though false positives were seen when working with subtype H5N2 due to cross reactivity of the polyclonal α-N1 antibody. RBC amplification was shown to increase the impedance signal change by more than 100% compared to the protocol without RBC biolabels. Experimental results also showed that RBC amplification was necessary for formulating a calibration curve for the biosensor. Virus attachment alone showed no linear correlation between virus concentration and impedance change with an R^2 value of 0.10 but after RBC amplification a linear correlation could be seen with an R^2 value of 0.83. The biosensor was experimentally shown to have a lower

detection limit of 10^3 EID_{50} ml^{-1} when using RBC amplification. RBC amplification did not allow for small standard deviation bars or a high R^2 value due to the relatively large size of the RBC compared to the virus. A single RBC may be bound by more than one virus, making it difficult to correlate virus concentration to impedance change after RBC amplification. Though the lower detection limit was the same as the previous biosensors, the new biosensor design offered much greater specificity than the previous protocol due to the use of a second antibody against N1.

Acknowledgments

This research was supported by a Grant from the USDA/NRI (Project #2008-35204-18662).

References

Amano, Y., Cheng, Q., 2005. Analytical and Bioanalytical Chemistry 381 (1), 156–164.
Bohinski, R.C., 2000. Journal of Chemical Education 77, 1460–1462.
Boltovets, P.M., Boyko, V.R., Kostikov, I.Y., Dyachenko, N.S., Snopok, B.A., Shirshov, Y.M., 2002. Journal of Virological Methods 105 (1), 141–146.
Burns, A., van der Mensbrugghe, D., Timmer, H., 2008. World Bank Report. 〈http://siteresources.worldbank.org/EXTAVIANFLU/Resources/EvaluatingAHIeconomics_2008.pdf〉 (accessed 05.03.12).
Cell Size Database, the subset of Animal Genome Size Database Available from: 〈http://www.genomesize.com/cellsize/birds.htm〉 (accessed 05.03.12) .
Charlton, B., Crossley, B., Hietala, S., 2009. Comparitive Immunology Microbiology and Infectious Diseases 32 (4), 341–350.
Chen, H., Gu, W., Cellar, N., Kennedy, R., Takayama, S., Meiners, J., 2008. Analytical Chemistry 80 (15), 6110–6113.
Duffy, D., McDonald, J., Schueller, O., Whitesides, G., 1998. Analytical Chemistry 70 (23), 4974–4984.
Ellis, J.S., Zambon, M.C., 2002. Reviews in Medical Virology 12 (6), 375–389.
Estmer-Nilsson, C., Abbas, S., Bennemo, M., Larsson, A., Hämäläinen, M.D., Frostell-Karlsson, A., 2010. Vaccine 28 (3), 759–766.
Goldstein, M.A., Tauraso, N.M., 1970. Applied Microbiology 19 (2), 290–294.
Horak, D., Babic, M., Mackova, H., Benes, M.J., 2007. Journal of Separation Science 30 (11), 1751–1772.
Lamb, R.A., Krug, R.M., 2001. In: Knipe, D.M., Howley, P.M. (Eds.), Field's Virology. Lippincott William & Wilkins Publisher, Philadelphia, PA, pp. 1487–1531.
Li , Y. , Hargis , B., Tung, S., Berghman, L., Bottje, W., Wang, R., Ye, Z., Varshney.M., Sriniwasan . B. , 2006. US Patent Applications 60/876,919.
Lindmark, R., Thorén-Tolling, K., Sjöquist, J., 1983. Journal of Immunological Methods 62 (1), 1–13.
MacKay, W.G., van Loon, A.M., Niedrig, M., Meijer, A., Lina, B., Niesters, H.G.M., 2008. Journal of Clinical Virology 42 (2), 194–197.
Murphy, B.R., Webster, R.G., 1996. In: Knipe, D.M., Howley, P.M. (Eds.), Field's Virology. Lippincott William & Wilkins Publisher, Philadelphia, PA., pp. 1397–1445.
Peduru Hewa, T.M., Tannock, G.A., Mainwaring, D.E., Harrison, S., Fecondo, J.V., 2009. Journal of Virological Methods 162 (1-2), 14–21.
Peiris, J.S., de Jong, M.D., Guan, Y., 2007. Clinical Microbiology Reviews 20 (2), 243–267.
Pejcic, B., De Marco, R., Parkinson, G., 2006. Analyst 131 (10), 1079–1090.
Sato, T., Serizawa, T., Okahata, Y., 1996. Biochimica et Biophysica Acta 1285 (1), 14–20.
Suarez, D.L., Schultz-Cherry, S., 2000. Developmental and Comparative Immunology 24 (2–3), 269–283.
Varshney, M., Li, Y., 2009. Biosensors and Bioelectronics 24 (10), 2951–2960.
Varshney, M., Li, Y., Srinivasan, B., Tung, S., 2007. Sensors and Actuators B 128 (1), 99–107.
Wang, R., Li, Y., Hargis, B., Tung, S., Bottje, W., Lassiter, K., Brewer, R., Sriniwasan, B., 2007. ASABE Paper No. 077112.
Wang, R., Wang, Y., Lassiter, K., Li, Y., Hargis, B., Tung, S., et al., 2009. Talanta 79 (2), 159–164.
WHO, 2011. 〈http://www.who.int/influenza/human_animal_interface/EN_GIP_20120224 CumulativeNumberH5N1cases.pdf〉 (accessed 24.02.12).
Xu, J., Suarez, D., Gottfried, D.S., 2007. Analytical and Bioanalytical Chemistry 389 (4), 1193–1199.
Yager, P., Edwards, T., Fu, E., Helton, K., Nelson, K., Tam, M.R., et al., 2006. Nature 442 (7101), 412–418.